

1 **A record of plume-induced plate rotation triggering seafloor spreading and**
2 **subduction initiation**

3
4 **Authors:** Douwe J.J. van Hinsbergen^{1*}, Bernhard Steinberger^{2,3}, Carl Guilmette⁴, Marco
5 Maffione^{1,5}, Derya Gürer^{1,6}, Kalijn Peters¹, Alexis Plunder^{1,7}, Peter J. McPhee¹, Carmen Gaina³,
6 Eldert L. Advokaat^{1,5}, Reinoud L.M. Vissers¹, and Wim Spakman¹

7 **Affiliations:**

8 ¹Department of Earth Sciences, Utrecht University, Princetonlaan 8A, 3584 CB Utrecht,
9 Netherlands

10 ²GFZ German Research Centre for Geosciences, Potsdam, Germany

11 ³Centre of Earth Evolution and Dynamics (CEED), University of Oslo, Norway

12 ⁴Département de Géologie et de Génie Géologique, Université Laval, Québec, QC G1K 7P4,
13 Canada

14 ⁵School of Geography, Earth and Environmental Sciences, University of Birmingham, B15 2TT,
15 UK

16 ⁶School of Earth and Environmental Sciences, University of Queensland, St Lucia, Queensland
17 4072, Australia

18 ⁷BRGM, F-45060, Orléans, France

19
20 *Correspondence to: Douwe J.J. van Hinsbergen (d.j.j.vanhinsbergen@uu.nl)

21
22 *Manuscript accepted for publication in Nature Geoscience, March 22, 2021*

24 **The formation of a global network of plate boundaries surrounding a mosaic of**
25 **lithospheric fragments was a key step in the emergence of Earth's plate tectonics. So far,**
26 **propositions for plate boundary formation are regional in nature but how plate boundaries**
27 **are being created over 1000s of km in short periods of geological time remains elusive.**
28 **Here, we show from geological observations that a >12,000 km long plate boundary formed**
29 **between the Indian and African plates around 105 Ma with subduction segments from the**
30 **eastern Mediterranean region to a newly established India-Africa rotation pole in the west-**
31 **Indian ocean where it transitioned into a ridge between India and Madagascar. We find no**
32 **plate tectonics-related potential triggers of this plate rotation and identify coeval mantle**
33 **plume rise below Madagascar-India as the only viable driver. For this, we provide a proof**
34 **of concept by torque balance modeling revealing that the Indian and African cratonic keels**
35 **were important in determining plate rotation and subduction initiation in response to the**
36 **spreading plume head. Our results show that plumes may provide a non-plate-tectonic**
37 **mechanism for large plate rotation initiating divergent and convergent plate boundaries**
38 **far away from the plume head that may even be an underlying cause of the emergence of**
39 **modern plate tectonics.**

40 The early establishment of plate tectonics on Earth was likely a gradual process that
41 evolved as the cooling planet's lithosphere broke into a mosaic of major fragments, separated by
42 a network of plate boundaries: seafloor spreading ridges, transform faults, and subduction
43 zones¹. The formation of spreading ridges and connecting transform faults is regarded as a
44 passive process, occasionally associated with rising mantle plumes². The formation of
45 subduction zones is less well understood. Explanations for subduction initiation often infer
46 spontaneous gravitational collapse of aging oceanic lithosphere², or relocations of subduction
47 zones due to intraplate stress changes in response to continental collisions with other continents,
48 oceanic plateaus, or arcs³. Mantle plumes have also been suggested as drivers for regional
49 subduction initiation, primarily based on numerical modeling⁴⁻⁶. But while such processes may
50 explain how plate tectonics evolves on a regional scale, they do not provide insight into the
51 geodynamic cause(s) for the geologically sudden (<10 My) creation of often long (>1000 km)
52 plate boundaries including new subduction zones⁷. Demonstrating the causes of plate boundary
53 formation involving subduction initiation using the geological record is challenging and requires
54 (i) establishing whether subduction initiation was spontaneous or induced; (ii) if induced,

55 constraining the timing and direction of incipient plate convergence; (iii) reconstructing the
56 entire plate boundary from triple junction to triple junction, as well as the boundaries of
57 neighboring plates, to identify collisions, subduction terminations, or mantle plume arrival that
58 may have caused stress changes driving subduction initiation. In this paper, we provide such an
59 analysis for an intra-oceanic subduction zone that formed within the Neotethys ocean around 105
60 Ma, to evaluate the driver of subduction initiation and plate boundary formation.

61

62 **Induced subduction initiation across the Neotethys Ocean**

63 Determining spontaneous versus induced subduction initiation is a particular complexity
64 in this analysis and requires geological records of both the upper and lower plates: in both cases,
65 subduction initiation corresponds with initial lower plate burial, whereas coeval or delayed
66 extension in the upper plate are contrasting diagnostics of spontaneous or forced subduction
67 initiation, respectively⁸. Initiation of lower plate burial can be dated through prograde mineral
68 growth in rocks of the incipient subduction plate contact, in so-called metamorphic soles⁸. The
69 timing of extension is inferred from spreading records in so-called supra-subduction zone (SSZ)
70 ophiolites^{8-10,11}. Such SSZ ophiolites have a chemical stratigraphy widely interpreted as having
71 formed at spreading ridges above a nascent subduction zones. Metamorphic sole protoliths
72 typically reveal that also the initial downgoing plate was of oceanic composition^{2,9}, and so
73 ophiolite belts with metamorphic soles demarcate fossil juvenile intra-oceanic subduction plate
74 boundaries.

75 Several SSZ ophiolite belts exist in the Alpine-Himalayan mountain belt, which formed
76 during the closure of the Neotethys Ocean^{12,13} (Fig. 1A). One of these ophiolite belts formed in
77 Cretaceous time and runs from the eastern Mediterranean region to Pakistan, across northern
78 Arabia. The timing of lower plate burial as well as upper plate extension have been constrained
79 in this ophiolite belt through detailed geochronological, petrological, and geochemical work.
80 Incipient lower plate burial has been dated through Lu/Hf prograde garnet growth ages of ~104
81 Ma in Oman as well as in the eastern Mediterranean region^{8,14}. Upper plate extension and SSZ
82 ophiolite spreading has been dated using magmatic zircon U/Pb ages and synchronous
83 metamorphic sole ⁴⁰Ar/³⁹Ar cooling ages and occurred at 96-95 Ma (Pakistan, Oman)^{15,16} to 92-
84 90 Ma (Iran, eastern Mediterranean region)¹⁷. The 8-14 Myr time delay between initial lower

85 plate burial and upper plate extension demonstrates that initiation of this subduction zone was
86 not spontaneous, but induced by far-field forcing⁸.

87 An initial ~E-W convergence direction at this subduction zone was constrained through
88 paleomagnetic analysis and detailed kinematic reconstruction of post-subduction initiation
89 deformation of the eastern Mediterranean region, Oman, and Pakistan, and was accommodated at
90 ~N-S striking trench segments^{13,18-20}. This is surprising: for hundreds of Ma, throughout the
91 Tethyan realm rifts and ridges formed breaking fragments off northern Gondwana in the south,
92 which accreted at subduction zones to the southern Eurasian margin in the north^{21,22}. The ~E-W
93 convergence that triggered ~105 Ma subduction initiation across the Neotethys ocean was thus
94 near orthogonal to the long-standing plate motions. To find this trigger we developed the first
95 comprehensive reconstruction of the entire ~12,000 km long plate boundary that formed at ~105
96 Ma and placed this in context of reconstructions of collisions and mantle plumes of the
97 Neotethyan realm.

98

99 **Geological reconstruction of plate boundary formation across the Neotethys**

100 The Cretaceous SSZ ophiolites that formed at the Cretaceous intra-Neotethyan
101 subduction zone in its juvenile stages are now found as klippen on intensely deformed orogenic
102 belts (Fig. 1A). These belts formed during subduction zone migration and collisions with the
103 continents of Greater Adria, Arabia, and India. We reconstructed these orogenic belts (Fig. 1)
104 and restored the Cretaceous ophiolites into their original configuration (Fig. 1C) (see Methods).

105 The westernmost geological record of the Cretaceous intra-Neotethyan subduction zone
106 is found in eastern Greece and western Turkey, where it ended in a trench-trench-trench triple
107 junction with subduction zones along the southern Eurasian margin¹⁸. From there, east-dipping
108 (in the west) and west-dipping (in the east) subduction segments followed the saw-toothed shape
109 of the Greater Adriatic and Arabian continental margins (Fig. 1C) and initiated close to it: rocks
110 of these margins already underthrust the ophiolites within 5-15 My after SSZ ophiolite
111 spreading^{14,23,24}, and continent-derived zircons have been found in metamorphic sole rocks²⁵.
112 Subduction segments that likely nucleated along ancient N-S and NE-SW trending fracture
113 zones, linked through highly oblique, north-dipping subduction zones that trended parallel to and
114 likely reactivated the pre-existing (hyper)extended passive margins (Fig. 1B, C)^{20,23}. Subducted

115 remnants of the Cretaceous intra-Neotethyan subduction are well-resolved in the present-day
116 mantle as slabs below the southeastern Mediterranean Sea, central Arabia and the west Indian
117 Ocean²⁶.

118 East of Arabia, we trace the intra-oceanic plate boundary to a NE-SW striking, NW-
119 dipping subduction zone between the Kabul Block and the west Indian passive margin. The 96
120 Ma Waziristan ophiolites of Pakistan formed above this subduction zone and were thrust
121 eastward onto the Indian continental margin^{13,16} (Fig. 1B, C). This part of the plate boundary
122 may have inverted a spreading ridge that formed between the Kabul Block and India in the Early
123 Cretaceous¹³. The Cretaceous intra-Neotethyan plate boundary may have been convergent to as
124 far south as the Amirante Ridge in the west Indian Ocean¹³, but there is no record of
125 contemporaneous subduction beyond there. Instead, the plate boundary became extensional and
126 developed a rift, and later a mid-oceanic ridge in the Mascarene Basin that accommodated
127 separation of India from Madagascar^{13,27,28} (Fig. 1B). The plate boundary ended in a ridge-ridge-
128 ridge triple junction with ridges bordering the Antarctic plate in the south Indian Ocean^{13,28} (Fig.
129 1B).

130 The newly formed Cretaceous plate boundary essentially temporarily merged a large part
131 of Neotethyan oceanic lithosphere between Arabia and Eurasia to the Indian plate. This plate was
132 >12,000 km long from triple junction to triple junction, and reached from 45°S to 45°N, with
133 4500 km of rift/ridge in the southeast and 7500 km of subduction zone in the northwest and with
134 a transition between the convergent and divergent segments, representing the India-Africa Euler
135 pole¹³, in the west Indian Ocean (Fig. 1B). Marine geophysical constraints show a ~4°
136 counterclockwise rotation of India relative to Africa about the west Indian Ocean Euler pole
137 during rifting preceding the ~83 Ma onset of oceanic spreading in the Mascarene Basin²⁷⁻²⁹,
138 associated with up to hundreds of km of ~E-W convergence across the Neotethys (Fig. 1D).

139 The neighboring plates of the intra-Neotethyan subduction zone at 105 Ma were thus
140 Africa and India. The African plate was mostly surrounded by ridges and had a complex
141 subduction plate boundary in the Mediterranean region³⁰. The Indian plate was surrounded by
142 ridge-transform systems in the south and east and by subduction in the north, and may have
143 contained rifts and ridges between the Indian continent and Eurasia^{13,28}. The Neotethys
144 lithosphere between Arabia-Greater Adria and Eurasia continued unbroken to the north-dipping

145 subduction zone that had already existed along the southern Eurasian margin since the
146 Jurassic^{31,32}; the spreading ridges that existed during Neotethys Ocean opening in the Permian-
147 Triassic (north of Arabia)³³, and Triassic-Jurassic (eastern Mediterranean region)²³ had already
148 subducted below Eurasia by 105 Ma^{19,33} (Fig. 1B, C).

149

150 **Identifying potential drivers of plate boundary formation**

151 Collisions, subduction relocations, or mantle plume arrivals around or within the Indian
152 or African plates are all candidate processes to explain plate boundary formation at 105 Ma. At
153 the northern boundary of between these plates and southern Eurasia, many collisions of
154 microcontinents and arcs occurred since the Paleozoic, but none started or ended around 105
155 Ma^{13,21-23,33-35}. Continental subduction and collision was ongoing in the central Mediterranean
156 region²³, but it is not evident how this or any other changes in subduction dynamics along the E-
157 W trending southern Eurasian margin would lead to E-W convergence in the Neotethys Ocean.
158 In the eastern Neotethys, a mid-Cretaceous collision of the intra-oceanic Woyla Arc with the
159 Sundaland continental margin led to a subduction polarity reversal initiating eastward subduction
160 below Sundaland³⁶, which is recorded in ophiolites on the Andaman Islands. There, metamorphic
161 sole rocks with ⁴⁰Ar/³⁹Ar hornblende cooling ages of 105-106 Ma, and likely coeval SSZ
162 ophiolite spreading ages³⁷ reveal that this subduction zone may have developed slab pull around
163 the same time as the Indian Ocean-western Neotethys plate boundary formed (Fig 1C). However,
164 eastward slab pull below Sundaland cannot drive E-W convergence in the Neotethys to the west,
165 and Andaman SSZ extension may well be an expression rather than the trigger of Indian plate
166 rotation. Hence, we find no viable plate tectonics-related driver of the ~105 Ma plate boundary
167 formation that we reconstructed here.

168 A key role, however, is possible for the only remaining geodynamic, non-plate-tectonic,
169 plate-motion driver in the region: a mantle plume. India-Madagascar continental breakup is
170 widely viewed^{13,27,37} as related to the ~94 Ma and younger formation of the Morondava Large
171 Igneous Province (LIP) on Madagascar³⁸ and southwest India³⁹. This LIP, however, started
172 forming ~10 Ma after initial plate boundary formation. To understand whether the plume may be
173 responsible for both LIP emplacement and plate boundary formation, we conduct explorative
174 torque-balance simulations of plume-lithosphere interaction.

175

176 **Mantle plumes driving plate boundary formation and subduction initiation**

177 Numerical simulations of plume-lithosphere interaction have already identified that
178 plume head spreading below the lithosphere leads to horizontal asthenospheric flow that exerts a
179 ‘plume push’ force on the base of the lithosphere, particularly in the presence of a cratonic
180 keel^{5,40,41}. Plume push may accelerate plates by several cm/yr⁴¹ and has been proposed as a
181 potential driver of subduction initiation⁵.

182 In many cases, including in the case of the Morondava LIP, LIP eruption and
183 emplacement shortly preceded continental breakup, but pre-break up rifting preceded LIP
184 emplacement by 10-15 Myr²⁷. This early rifting typically is interpreted to indicate that the plume
185 migrated along the base of the lithosphere into a pre-existing rift that formed independently of
186 plume rise²⁷. However, in numerical simulations dynamic uplift⁴² and plume push⁴¹ already start
187 to accelerate plates 10-15 Myr before the plume head reaches the base of the lithosphere and
188 emplaces the LIP. Numerical simulations thus predict the observed delay between plume push,
189 as a driver for early rifting and subduction initiation, and LIP eruption and emplacement.

190 Here, we add to these plume-lithosphere coupling experiments by conducting proof-of-
191 concept torque-balance simulations particularly exploring why the observed India-Africa Euler
192 pole is so close to the plume head such that the associated plate rotation between Africa and
193 India caused E-W convergence in the Neotethys. We performed semi-analytical computations,
194 including both the Indian and African plates at ~105 Ma, and assess the influence of cratonic
195 keels on the position of the India-Africa Euler pole (Fig. 2, see Methods).

196 In our computations without cratonic keels, plume push under Madagascar/India caused
197 counterclockwise rotation of India versus Africa, but about an Euler pole situated far north of
198 Arabia, (Fig. 2A) without inducing significant E-W convergence within the Neotethys. However,
199 in experiments that include keels of the Indian and African cratonic lithosphere, which are
200 strongly coupled to the sub-asthenospheric mantle, the computed Euler pole location is shifted
201 southward towards the Indian continent, inducing E-W convergence along a larger part of the
202 plate boundary within the Neotethys Ocean (Fig. 2B).

203 Convergence of up to several hundreds of km, sufficient to induce self-sustaining
204 subduction²⁷, is obtained if plume material is fed into – and induced flow is confined to – a 200
205 km thick weak asthenospheric layer. The thinner this layer is, the further the plume head spreads,
206 and pushes the plate. The modern Indian cratonic root used in our computations has likely eroded
207 considerably during interaction with the ~70-65 Ma Deccan plume⁴³. India may have had a
208 thicker and/or laterally more extensive cratonic root at ~105 Ma than modeled here which would
209 further enhance coupling of the lithosphere and the sub-asthenospheric mantle. Furthermore, an
210 Euler pole close to India and a long convergent boundary to the north requires much weaker
211 coupling in the northern (oceanic) part of the India plate (Fig. 2). In this case, results remain
212 similar as long as the plume impinges near the southern part of the western boundary of
213 continental India.

214 An order of magnitude estimate of the maximum plume-induced stresses, assuming no
215 frictional resistance at other plate boundaries, is obtained from the rising force of $\sim 1.5 \cdot 10^{20}$ N of
216 a plume head with 1000 km diameter and density contrast 30 kg/m^3 . If half of this force acts on
217 the India plate and with a lever arm of 4000 km, this corresponds to a torque of $3 \cdot 10^{26}$ Nm. Once,
218 at the onset of rifting, ridge push is established as an additional force in the vicinity of the plume,
219 we estimate that this number may increase by up to a few tens of per cent. This torque can be
220 balanced at the convergent boundary (length ~ 5000 km, plate thickness ~ 100 km) involving
221 stresses of ~ 240 MPa, much larger than estimates of frictional resistance between subducting and
222 overriding plates that are only of the order of tens of MPa⁴⁴. For this estimate, we neglect any
223 frictional resistance at the base of the plate and at any other plate boundary – essentially
224 considering the plate as freely rotating above a pinning point. This is another endmember
225 scenario, as opposed to our above convergence estimate, where we had considered friction at the
226 plate base but neglected it at all plate boundaries. Therefore, the estimate of 240 MPa may be
227 considered as an upper bound but being compressive and oriented in the right direction it shows
228 the possibility of subduction initiation as has occurred in reality along the likely weakened
229 passive margin region of Arabia and Greater Adria. Moreover, the plume-induced compressive
230 stresses may have added to pre-existing compressive stresses, in particular due to ridge-push
231 around the African and Indian plates. Such additional compressive stresses may contribute to
232 shifting the Euler pole further south, closer to the position reconstructed in Fig. 1.

233 Subduction became self-sustained ~8-12 Ma after its initiation, as marked by the 96-92
234 Ma age of SSZ spreading^{15,17}: inception of this spreading shows that subduction rates exceeded
235 convergence rates, and reconstructed SSZ spreading rates were an order of magnitude higher¹⁵
236 than Africa-Arabia or Indian absolute plate motions^{41,45} signaling slab roll-back, i.e. self-
237 sustained subduction^{20,46}. Numerical models suggest that self-sustained subduction may start
238 after ~50-100 km of induced convergence⁷, corresponding to ~1° of India-Africa rotation
239 between ~105 and ~96-92 Ma. Subsequent east and west-dipping subduction segments (Fig. 1)
240 may have contributed to and accelerated the India-Africa/Arabia rotation, driving the
241 propagation of the Euler pole farther to the south (compare Fig. 2A, C).

242

243 **Mantle plumes as an initiator of plate tectonics?**

244 Previously, numerical modeling has shown that mantle plumes may trigger circular
245 subduction initiation around a plume head⁴, where local plume-related convection may drive
246 subduction of thermally weakened lithosphere. This subduction would propagate through slab
247 roll-back and may have started the first subduction features on Earth⁴. 3D convective models do
248 produce a global network of plate boundaries^{47,48} but the role of plumes in initiating new
249 subduction zones within this network is unclear. Here, we have provided the first evidence that
250 plume rise formed a >12,000 km long plate boundary composed of both convergent and
251 divergent segments. Our documented example is Cretaceous in age but geological observations
252 showing a general temporal overlap between LIP emplacement and formation of SSZ ophiolite
253 belts over more than a billion years⁴⁹ suggest that plume rise is a key driving factor in the
254 formation of subduction plate boundaries. Because mantle plumes are thought to be also
255 common features on planets without plate tectonics, such as Mars and Venus⁵⁰, they may have
256 played a vital role in the emergence of modern style plate tectonics on Earth. That plumes may
257 have been key for the evolution of plate tectonics on Earth, as we suggest, but apparently
258 insufficient on Mars and Venus, provides a new outlook on understanding the different planetary
259 evolutions.

260

261 **Acknowledgments:** DJJvH, MM, DG, AP, and ELA were funded through European Research
262 Council Starting Grant 306810 (SINK) to DJJvH. DJJvH, KP and PJMcP were funded

263 through Netherlands Organization for Scientific Research (NWO) Vidi grant 864.11.004
264 to DJJvH. DJJvH acknowledges Netherlands Organization for Scientific Research
265 (NWO) Vici grant 865.17.001. BS and CGa received funding from the Research Council
266 of Norway through its Centres of Excellence funding scheme, project number 223272.
267 BS received additional funding from the innovation pool of the Helmholtz Association
268 through the “Advanced Earth System Modelling Capacity (ESM)” activity. CG was
269 funded through Discovery Grant (RGPIN-2014-05681) from the National Science and
270 Engineering Research Council of Canada. We thank Inge Loes ten Kate and Debaditya
271 Bandyopadhyay for discussion, and Fabio Capitanio, Dietmar Müller, and an anonymous
272 reviewer for their constructive comments.

273

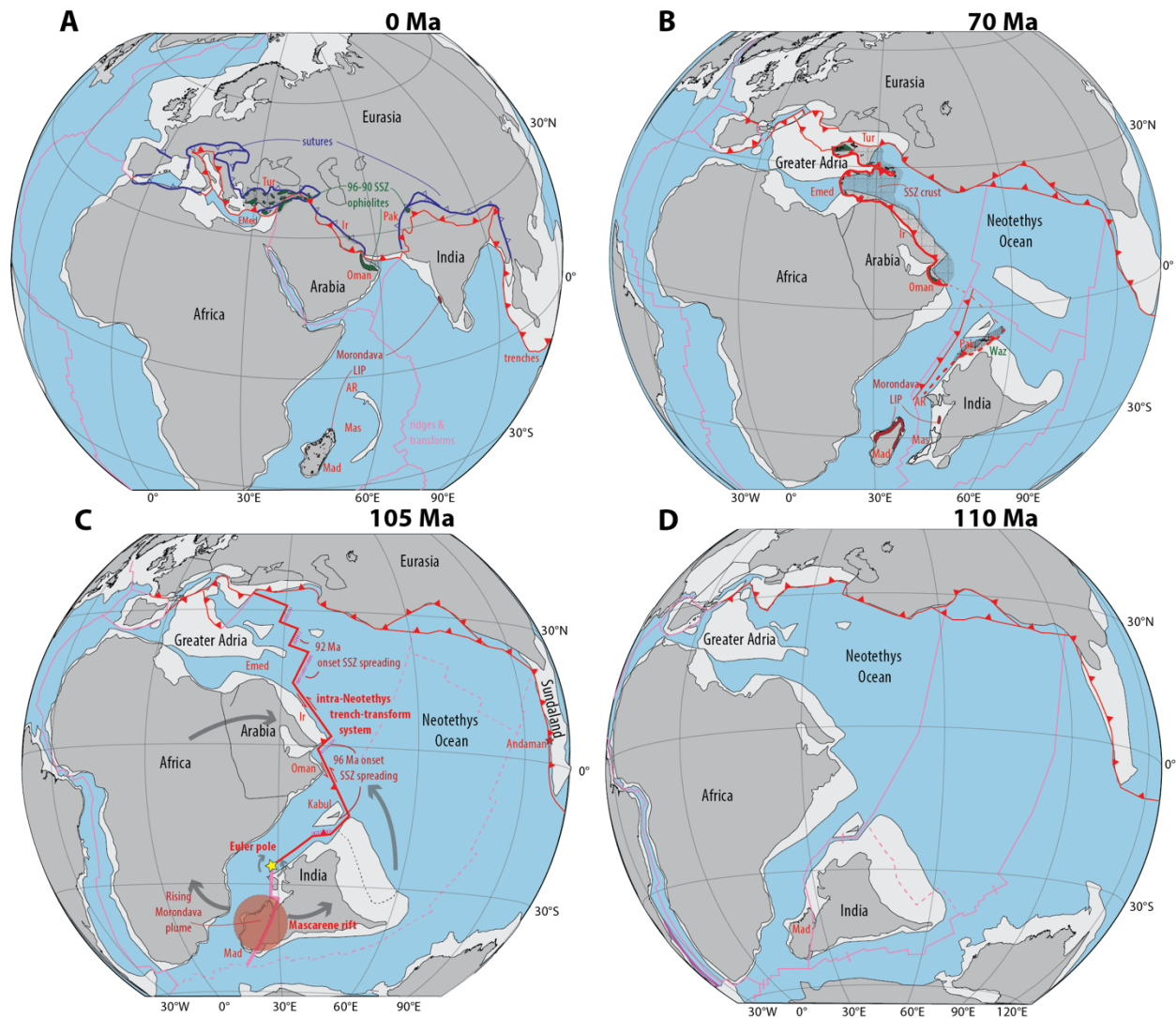
274 **Author contributions:** DJJvH, BS, WS designed research. DJJvH, CGu, MM, DG, KP, AP,
275 PJmcP, CGa, ELA and RLMV developed the kinematic reconstruction; BS performed
276 modelling; DJJvH, BS, CGu, WS wrote the paper, all authors made corrections and edits.

277

278 **Competing interests:** All authors declare no competing interests.

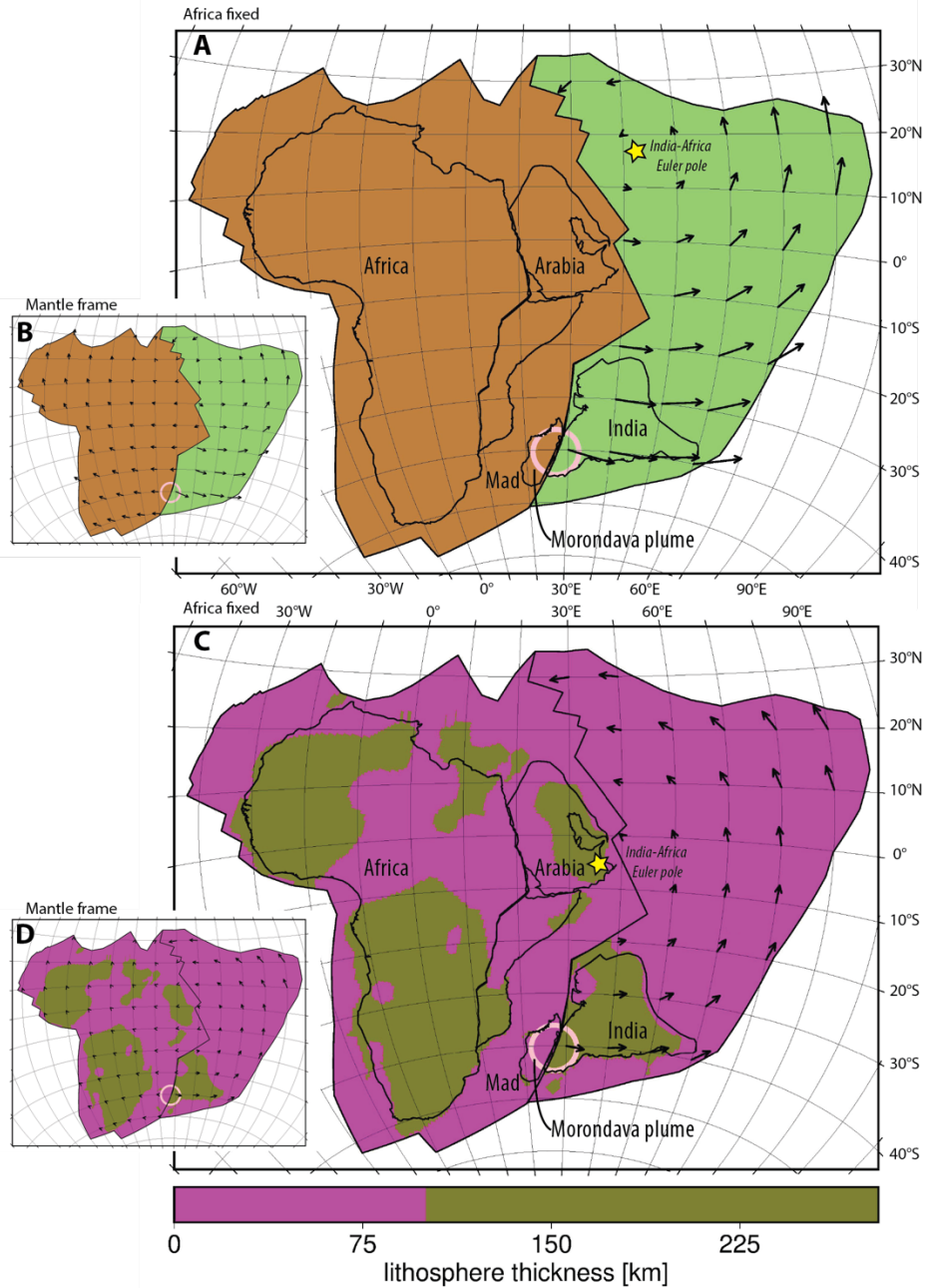
279

280



281
 282 **Fig. 1.** Plate kinematic reconstructions of the Neotethys Ocean and surrounding continents at A)
 283 the present-day; B) 70 Ma, corresponding to the time that most of the Neotethyan intra-oceanic
 284 subduction zone had terminated due to arrival of the India, Africa-Arabia, and the Greater Adria
 285 margin in the trench; C) 105 Ma, corresponding to the timing of intra-Neotethyan subduction
 286 initiation and D) 110 Ma, just before intra-Neotethyan subduction initiation. An Euler pole
 287 situated in the Indian Ocean north of Madagascar (yellow star) indicates the division between the
 288 compressional plate boundary segment (the intra-Neotethys trench) and the extensional segment
 289 (the incipient Mascarene rift connected to the mid-ocean ridge between Africa and Antarctica).
 290 Rotation around this pole, and the related intra-Neotethyan subduction initiation, are interpreted
 291 here to result from the rise and push of the Morondava mantle plume. See text for further
 292 explanation, and Methods for the plate reconstruction approach and sources of detailed

293 restorations. Dark grey areas outline modern continents; light-grey areas indicate thinned
294 continental margins and microcontinents. Grey arrows indicate approximate rotational motion in
295 a mantle reference frame⁴⁵ around the Amiranter Euler pole. AR = Amiranter Ridge; Emed =
296 Eastern Mediterranean Region; Ir = Iran; LIP = Large Igneous Province; Mad = Madagascar;
297 Mas = Mascarene Basin; Pak = Pakistan, Tur = Turkey; Waz = Waziristan Ophiolite.



298

299 **Fig. 2.** The computed total displacement, induced by the Morondava plume (pink circle) for the
 300 restored ~105 Ma plate configuration (Fig. 1C) for plates without (A, B) and with (C, D) African
 301 and Indian cratonic keels, in an Africa-fixed (A, C), or mantle reference frame⁴⁵ (B, D) (see
 302 Methods). It is assumed that, compared to a case with no lateral variations, the drag force due to
 303 the plate moving over the mantle is increased by a factor of ten wherever reconstructed
 304 lithosphere thickness exceeds 100 km (brown areas) and reduced to one tenth of the drag force

305 wherever it is less than 100 km thick. The India craton hence nearly “pins” the India plate, such
306 that its northern part moves in the opposite direction to the plume-induced push. Computation
307 assumes torque balance between plume push and shearing over asthenosphere; frictional
308 resistance at plate boundaries is neglected and computed convergence of several hundred km at
309 the northern end of the plate boundary is a maximum estimate. Ten degree grid spacing;
310 locations of plates, lithosphere thickness and the plume are reconstructed in a slab-fitted mantle
311 reference frame⁴⁵.

312

313 **Methods:** *Kinematic reconstruction* – The kinematic restoration of Neotethyan intra-
314 oceanic subduction was made in GPlates plate reconstruction software (www.gplates.org)⁵¹.
315 First, we systematically restored stable plates using marine geophysical data from the Atlantic
316 and Indian Ocean, and then restored continental margin deformation that occurred following the
317 arrival of continental lithosphere below the oceanic lithosphere preserved as ophiolites. These
318 restorations are based on a systematic reconstruction protocol, based on magnetic anomalies and
319 fracture zones of present-day sea floor and geophysical constraints on pre-drift extension in
320 adjacent passive continental margins²³, followed by kinematic restoration of post-obduction
321 orogenic deformation using structural geological constraints on continental extension, strike-slip
322 deformation, and shortening, and paleomagnetic constraints on vertical axis rotations. We then
323 restored pre-emplacement vertical axis microplate rotations^{52,53}, as well as paleo-orientations of
324 the SSZ spreading ridges at which the ophiolitic crust formed¹⁸⁻²⁰. The reconstruction shown in
325 Fig. 1B compiles kinematic restorations for the eastern Mediterranean region²³, Iran⁵⁴, Oman²⁰,
326 Pakistan¹³, and the Himalaya³⁴. Ophiolites interpreted to be part of the Cretaceous subduction
327 system include the 96-90 Ma, Cretaceous ophiolites exposed in SE Greece, Anatolia, Cyprus,
328 Syria, and Iraq, the Neyriz ophiolite of Iran, the Semail ophiolite in Oman, and the Waziristan-
329 Khost ophiolite in Pakistan and Afghanistan^{15-17,55}. The Jurassic ophiolite belts of northern
330 Turkey and Armenia⁵⁶⁻⁵⁸ and the late Cretaceous (<80 Ma) Kermanshah ophiolite of Iran⁵⁹ are
331 not included and are instead interpreted to have formed along the southern Eurasian margin²³.
332 The Masirah Ophiolite of East Oman⁶⁰ and the uppermost Cretaceous Bela, Muslim Bagh, and
333 Kabul-Altimur ophiolites of Pakistan and Afghanistan^{61,62} are interpreted to reflect oblique latest
334 Cretaceous to Paleogene India-Arabia convergence¹³ and are also unrelated to the event studied

335 here. Restoration of intra-oceanic subduction prior to the arrival of the continental margins used
336 paleomagnetic data from the ophiolites of Oman, Syria, Cyprus, and Turkey that constrain
337 vertical axis rotations, as well as the orientation of sheeted dyke following cooling after
338 intrusion^{18-20,52,53} as proxy for original ridge and intra-oceanic trench orientations. These
339 paleomagnetic data systematically revealed N-S to NW-SE primary sheeted dyke orientations¹⁸⁻
340 ^{20,52,53}. Because the ages of the SSZ ophiolites in the Neotethyan belt do not laterally progress,
341 spreading must have occurred near-orthogonal to the associated trench, which must thus also
342 have been striking N-S to NE-SW, as shown in the reconstruction of Fig. 1.

343 How far the Indian plate continued northwards around 105 Ma is subject to ongoing
344 debate. On the one hand, the northern Indian continental margin has been proposed to have rifted
345 off India sometime in the Cretaceous^{34,63}, but recent paleomagnetic data suggest that this process
346 occurred in the late Cretaceous, well after 100 Ma⁶⁴. Others inferred that the north Indian
347 continent had a passive margin contiguous with oceanic Neotethyan lithosphere since the middle
348 Jurassic or before and continued to a subduction zone below the SSZ ophiolites found in the
349 Himalayan suture zone and the Kohistan arc^{35,65,66}. Sedimentary and paleomagnetic data
350 demonstrate that these ophiolites formed adjacent to the Eurasian margin in the Early
351 Cretaceous⁶⁷, although they may have migrated southward during slab roll-back in the Late
352 Cretaceous³⁵. Recent paleomagnetic data have shown that a subduction zone may have existed
353 within the Neotethys to the west of the Andaman Islands, above which the West Burma Block
354 would have been located (Figure 1)⁶⁸. Our reconstruction of the eastern Neotethys may thus be
355 oversimplified. However, the geological record of the West Burma Block shows that this
356 subduction zone already existed as early as 130 Ma, and E-W trending until well into the
357 Cenozoic⁶⁸, and we see no reason to infer that changes in the eastern Neotethys contributed to
358 the plate boundary formation discussed here. Some have speculated that the West Burma
359 subduction zone would have been connected to a long-lived, equatorial subduction zone within
360 the Neotethys all along the Indian segment that would already have existed in the Early
361 Cretaceous⁶⁹: this scenario remains unconstrained by paleomagnetic data, and is inconsistent
362 with sediment provenance data from the Himalaya and overlying ophiolites³⁵. In summary, the
363 Indian plate around 105 Ma continued far into the Neotethyan realm, and the India-Africa
364 rotation is a likely driver of E-W convergence sparking subduction initiation close to the
365 northern Gondwana margin purported in Figure 1.

366 *Torque balance modeling* – Forces considered here include (i) the push due to plume-
367 induced flow in the asthenosphere and (ii) the drag due to shear flow between the moving plate
368 and a deeper mantle at rest (Fig. S1). In the first case, we disregard any lateral variations. Plume-
369 induced flow is treated as Poiseuille flow, i.e. with parabolic flow profile, in an asthenospheric
370 channel of thickness h_c , radially away from the plume stem. Since at greater distance plume-
371 induced flow will eventually not remain confined to the asthenosphere, we only consider it to a
372 distance 2400 km, in accord with numerical results⁴¹, and consistent with the finding that there is
373 a transition from dominantly pressure-driven Poiseuille flow at shorter wavelengths to
374 dominantly shear-driven Couette flow at length scales approximately exceeding mantle
375 depth^{70,71}. With v_0 the velocity in the center of the channel at a distance d from the plume stem
376 the total volume flux rate is $2/3 \cdot v_0 \cdot 2\pi d \cdot h_c$ (here neglecting the curvature of the Earth surface
377 for simplicity). Its time integral is equal to the volume of the plume head with radius estimated⁷²
378 to be about $r_p=500$ km, with considerable uncertainty. That is, integration is done over a time
379 interval until the entire plume head volume has flown into the asthenospheric channel. Hence the
380 corresponding displacement vector in the center of the channel is

$$\mathbf{x}_{plu} = \int_{\Delta t} v_0 dt \cdot \mathbf{e}_r = \frac{r_p^3}{d \cdot h_c} \cdot \mathbf{e}_r$$

381
382 where \mathbf{e}_r is the unit vector radially away from the plume (red arrows in Extended Data Fig. 1).
383 Because of the parabolic flow profile, the vertical displacement gradient at the top of the channel
384 is

$$2 \cdot \frac{\mathbf{x}_{plu}}{0.5 \cdot h_c} = 2 \cdot \int_{\Delta t} v_0 dt \cdot \frac{1}{0.5 \cdot h_c} \cdot \mathbf{e}_r = \frac{4r_p^3}{d \cdot h_c^2} \cdot \mathbf{e}_r.$$

385
386 Viscosity is defined such that the force per area is equal to viscosity times the radial gradient of
387 horizontal velocity. Hence the time integral of torque on the plate is

$$\mathbf{T}_{plu} = \frac{4\eta_0}{h_c} \int_A \mathbf{r} \times \mathbf{x}_{plu} dA = \frac{4\eta_0 r_p^3}{d \cdot h_c^2} \int_A \mathbf{r} \times \mathbf{e}_r dA$$

388

389 where η_0 is viscosity in the channel and \mathbf{r} is the position vector. \mathbf{T}_{plu} is balanced by the time-
 390 integrated torque \mathbf{T}_{pla} of the plate rotating an angle $\boldsymbol{\omega}$ over the underlying mantle. With plate
 391 displacement vectors $\mathbf{x}_{pla} = \boldsymbol{\omega} \times \mathbf{r}$ (black arrows in Fig. S1) we obtain

$$\mathbf{T}_{pla} = -\frac{\eta_0}{h_s} \int_A \mathbf{r} \times \mathbf{x}_{pla} dA = -\frac{\eta_0}{h_s} \int_A \mathbf{r} \times (\boldsymbol{\omega} \times \mathbf{r}) dA$$

392
 393 Here h_s is an effective thickness of the layer over which shearing occurs, which is calculated
 394 below for a stratified viscosity structure, i.e. laterally homogeneous coupling of plate and mantle
 395 and which we will set equal to h_c for simplicity. Specifically, with \mathbf{T}_x being the time-integrated
 396 torque acting on a plate rotating an angle ω_0 around the x-axis

$$\mathbf{T}_x = -\frac{\omega_0 \eta_0}{h_s} \int_A \mathbf{r} \times (\mathbf{e}_x \times \mathbf{r}) dA,$$

397
 398 and \mathbf{T}_y and \mathbf{T}_z defined in analogy, the torque balance equation can be written

$$\mathbf{T}_{plu} = \frac{\omega_x}{\omega_0} \cdot \mathbf{T}_x + \frac{\omega_y}{\omega_0} \cdot \mathbf{T}_y + \frac{\omega_z}{\omega_0} \cdot \mathbf{T}_z$$

399
 400 ω_0 cancels out when \mathbf{T}_x , \mathbf{T}_y and \mathbf{T}_z are inserted. Integrals used to compute these torques only
 401 depend on plate geometry, η_0 cancels out in the torque balance, and we can solve for the rotation
 402 angle vector $\boldsymbol{\omega}$ simply by a 3 x 3 matrix inversion. In the more general case, where we do not set
 403 h_s and h_c equal, $\boldsymbol{\omega}$ is scaled by a factor h_s/h_c .

404 If a plate moves over a mantle where viscosity varies with depth, then the force per area
 405 F/A should be the same at all depths, and the radial gradient of horizontal velocity $dv/dz = F/A \cdot$
 406 $1/\eta(z)$. If we assume that the deep mantle is at rest (i.e. it moves slowly compared to plate
 407 motions), we further find that plate motion is

$$v_0 = \int_{z_0}^{z(\eta_{\max})} \frac{dv}{dz} dz = \frac{F}{A} \int_{z_0}^{z(\eta_{\max})} \frac{1}{\eta(z)} dz =: \frac{F}{A} \frac{h_s}{\eta_0} \quad (1)$$

408
 409 The integration is done from the base of the lithosphere z_0 to the depth where the approximation
 410 of the ‘‘mantle at rest’’ is probably the most closely matched, i.e. we choose the viscosity

411 maximum. The last equality is according to the definition of the effective layer thickness,
412 whereby η_0 is the viscosity just below the lithosphere. Solving this equation for h_s for the
413 viscosity structure in Extended Data Fig. 2 and a 100 km thick lithosphere gives $h_s=203.37$ km.

414 The plume location at 27.1°E, 40.4° S, is obtained by rotating the center of the
415 corresponding LIP at 46° E, 26° S and an age 87 Ma (adopted from Doubrovine et al.⁷³) in the
416 slab-fitted mantle reference frame⁴⁵, in which also the plate geometries at 105 Ma are
417 reconstructed.

418 Results for this case (Fig. 2A) show that a plume pushing one part of a plate may induce
419 a rotation of that plate, such that other parts of that plate may move in the opposite direction. A
420 simple analog is a sheet of paper pushed, near its bottom left corner, to the right: Then, near the
421 top left corner, the sheet will move to the left. With two sheets (plates) on either side, local
422 divergence near the bottom (near the plume) may turn into convergence near the top (at the part
423 of the plate boundary furthest away from the plume). The length of that part of the plate
424 boundary, where convergence is induced may increase, if one plate is nearly “pinned” at a hinge
425 point slightly NE of the plume, perhaps due to much stronger coupling between plate and mantle.
426 At the times considered here ~105 My ago, the Indian continent, where coupling was presumably
427 stronger, was in the southern part of the Indian plate, whereas in its north, there was a large
428 oceanic part, with presumably weaker coupling. Hence the geometry was indeed such that
429 convergence could be induced along a longer part of the plate boundary.

430 In the second case, we therefore consider lateral variations in the coupling between plate
431 and mantle, corresponding to variations in lithosphere thickness and/or asthenosphere viscosity,
432 by multiplying the drag force (from the first case) at each location with a resistance factor. This
433 factor is a function of lithosphere thickness reconstructed at 105 Ma. On continents, thickness
434 derived from tomography⁷⁴ with slabs removed⁷⁵ is simply backward-rotated. In the oceans, we
435 use thickness [km] = 10 · (age [Ma] - 105)^{0.5} with ages from present-day Earthbyte age grid
436 version 3.6, i.e. accounting for the younger age and reduced thickness at 105 Ma, besides
437 backward-rotating. To determine the appropriate rotation, the lithosphere (in present-day
438 location) is divided up into India, Africa, Arabia, Somalia and Madagascar (paleo-)plates and
439 respective 105 Ma finite rotations from van der Meer et al.⁴⁵ are applied. For the parts of the
440 reconstructed plates where thickness could not be reconstructed in this way – often, because this

441 part of the plate has been subducted – we first extrapolate thickness up to a distance $\sim 2.3^\circ$, and
442 set the thickness to a default value of 80 km for the remaining part. Reconstructed thickness is
443 shown in Extended Data Fig. 4. For the resistance factor as a function of lithosphere thickness
444 we use two models: Firstly, we use a continuous curve (Extended Data Fig. 3) according to eq.
445 (1)

$$\frac{F}{A} = \frac{v_0}{\int_{z_0}^{z(\eta_{\max})} \frac{1}{\eta(z)} dz}. \quad (2)$$

446
447 with the mantle viscosity model in Extended Data Fig. 2 combined with variable lithosphere
448 thickness z_0 . However, this causes only a minor change in the plate rotations (Extended Data Fig.
449 4 compared to Fig. 2B). Hence, we also use a stronger variation, further explained in the caption
450 of Fig 2 and with results shown in Fig. 2C and D.

451

452 **Data availability**

453 GPlates files with reconstructions used to draft Figure 1 are provided at
454 https://figshare.com/articles/dataset/van_Hinsbergen_NatureGeo_2021_GPlates_zip/13516727.

455

456 **Code availability**

457 All codes used in the geodynamic modeling in this study are available at
458 https://figshare.com/articles/software/van_Hinsbergen_etal_NatureGeo_2021_geodynamics_package/13635089.

460

461

462 **References:**

- 463 1 Lenardic, A. The diversity of tectonic modes and thoughts about transitions between them. *Philosophical*
464 *Transactions of the Royal Society A: Mathematical, Physical and Engineering Sciences* **376**, 20170416
465 (2018).
- 466 2 Stern, R. J. Subduction initiation: spontaneous and induced. *Earth and Planetary Science Letters* **226**, 275-
467 292, doi:10.1016/s0012-821x(04)00498-4 (2004).
- 468 3 Hall, C. E., Gurnis, M., Sdrolias, M., Lavier, L. L. & Müller, R. D. Catastrophic initiation of subduction
469 following forced convergence across fracture zones. *Earth and Planetary Science Letters* **212**, 15-30,
470 doi:10.1016/s0012-821x(03)00242-5 (2003).
- 471 4 Gerya, T. V., Stern, R. J., Baes, M., Sobolev, S. V. & Whattam, S. A. Plate tectonics on the Earth triggered
472 by plume-induced subduction initiation. *Nature* **527**, 221-225, doi:10.1038/nature15752 (2015).
- 473 5 Pusok, A. E. & Stegman, D. R. The convergence history of India-Eurasia records multiple subduction
474 dynamics processes. *Science Advances* **6**, eaaz8681 (2020).
- 475 6 Baes, M., Sobolev, S., Gerya, T. & Brune, S. Plume-Induced Subduction Initiation: Single-Slab or Multi-
476 Slab Subduction? *Geochemistry, Geophysics, Geosystems* **21**, e2019GC008663 (2020).
- 477 7 Gurnis, M., Hall, C. & Lavier, L. Evolving force balance during incipient subduction. *Geochemistry,*
478 *Geophysics, Geosystems* **5**, doi:10.1029/2003gc000681 (2004).
- 479 8 Guilmette, C. *et al.* Forced subduction initiation recorded in the sole and crust of the Semail Ophiolite of
480 Oman. *Nature Geoscience* **11**, 688-695 (2018).
- 481 9 Stern, R. J. & Gerya, T. Subduction initiation in nature and models: A review. *Tectonophysics*,
482 doi:10.1016/j.tecto.2017.10.014 (2017).
- 483 10 Agard, P. *et al.* Plate interface rheological switches during subduction infancy: Control on slab penetration
484 and metamorphic sole formation. *Earth and Planetary Science Letters* **451**, 208-220 (2016).
- 485 11 van Hinsbergen, D. J. J. *et al.* Dynamics of intraoceanic subduction initiation: 2. Suprasubduction zone
486 ophiolite formation and metamorphic sole exhumation in context of absolute plate motions. *Geochemistry,*
487 *Geophysics, Geosystems* **16**, 1771-1785, doi:10.1002/2015gc005745 (2015).
- 488 12 Dilek, Y. & Furnes, H. Ophiolite genesis and global tectonics: Geochemical and tectonic fingerprinting of
489 ancient oceanic lithosphere. *Geological Society of America Bulletin* **123**, 387-411, doi:10.1130/b30446.1
490 (2011).
- 491 13 Gaina, C., van Hinsbergen, D. J. J. & Spakman, W. Tectonic interactions between India and Arabia since
492 the Jurassic reconstructed from marine geophysics, ophiolite geology, and seismic tomography. *Tectonics*
493 **34**, 875-906, doi:10.1002/2014tc003780 (2015).
- 494 14 Pourteau, A. *et al.* Thermal evolution of an ancient subduction interface revealed by Lu–Hf garnet
495 geochronology, Halilbağ Complex (Anatolia). *Geoscience Frontiers* **10**, 127-148,
496 doi:10.1016/j.gsf.2018.03.004 (2019).
- 497 15 Rioux, M. *et al.* Synchronous formation of the metamorphic sole and igneous crust of the Semail ophiolite:
498 New constraints on the tectonic evolution during ophiolite formation from high-precision U–Pb zircon
499 geochronology. *Earth and Planetary Science Letters* **451**, 185-195 (2016).
- 500 16 Robinson, J., Beck, R., Gnos, E. & Vincent, R. K. New structural and stratigraphic insights for
501 northwestern Pakistan from field and Landsat Thematic Mapper data. *Geological Society of America*
502 *Bulletin* **112**, 364-374, doi:10.1130/0016-7606(2000)112<364:Nsasif>2.0.Co;2 (2000).
- 503 17 Parlak, O. The tauride ophiolites of Anatolia (Turkey): A review. *Journal of Earth Science* **27**, 901-934,
504 doi:10.1007/s12583-016-0679-3 (2016).
- 505 18 van Hinsbergen, D. J. J. *et al.* Tectonic evolution and paleogeography of the Kırşehir Block and the Central
506 Anatolian Ophiolites, Turkey. *Tectonics* **35**, 983-1014, doi:10.1002/ (2016).
- 507 19 Maffione, M., van Hinsbergen, D. J. J., de Gelder, G. I. N. O., van der Goes, F. C. & Morris, A. Kinematics
508 of Late Cretaceous subduction initiation in the Neo-Tethys Ocean reconstructed from ophiolites of Turkey,
509 Cyprus, and Syria. *Journal of Geophysical Research: Solid Earth* **122**, 3953-3976,
510 doi:10.1002/2016jb013821 (2017).
- 511 20 van Hinsbergen, D. J., Maffione, M., Koornneef, L. M. & Guilmette, C. Kinematic and paleomagnetic
512 restoration of the Semail ophiolite (Oman) reveals subduction initiation along an ancient Neotethyan
513 fracture zone. *Earth and Planetary Science Letters* **518**, 183-196 (2019).
- 514 21 Torsvik, T. H. & Cocks, L. R. M. *Earth history and palaeogeography*. 317 (Cambridge University Press,
515 2017).

516 22 Wan, B. *et al.* Cyclical one-way continental rupture-drift in the Tethyan evolution: Subduction-driven plate
517 tectonics. *Science China Earth Sciences*, 1-12 (2019).

518 23 van Hinsbergen, D. J. J. *et al.* Orogenic architecture of the Mediterranean region and kinematic
519 reconstruction of its tectonic evolution since the Triassic. *Gondwana Research* **81**, 79-229 (2020).

520 24 Warren, C. J., Parrish, R. R., Waters, D. J. & Searle, M. P. Dating the geologic history of Oman's Semail
521 ophiolite: insights from U-Pb geochronology. *Contributions to Mineralogy and Petrology* **150**, 403-422,
522 doi:10.1007/s00410-005-0028-5 (2005).

523 25 Güngör, T. *et al.* Kinematics and U-Pb zircon ages of the sole metamorphics of the Marmaris Ophiolite,
524 Lycian Nappes, Southwest Turkey. *International Geology Review* **61**, 1124-1142 (2019).

525 26 van der Meer, D. G., van Hinsbergen, D. J. J. & Spakman, W. Atlas of the underworld: Slab remnants in
526 the mantle, their sinking history, and a new outlook on lower mantle viscosity. *Tectonophysics* **723**, 309-
527 448, doi:10.1016/j.tecto.2017.10.004 (2018).

528 27 Buitter, S. J. & Torsvik, T. H. A review of Wilson Cycle plate margins: A role for mantle plumes in
529 continental break-up along sutures? *Gondwana Research* **26**, 627-653 (2014).

530 28 Gibbons, A. D., Whittaker, J. M. & Müller, R. D. The breakup of East Gondwana: Assimilating constraints
531 from Cretaceous ocean basins around India into a best-fit tectonic model. *Journal of Geophysical*
532 *Research: Solid Earth* **118**, 808-822, doi:10.1002/jgrb.50079 (2013).

533 29 Gaina, C., Müller, R. D., Brown, B., Ishihara, T. & Ivanov, S. Breakup and early seafloor spreading
534 between India and Antarctica. *Geophysical Journal International* **170**, 151-169, doi:10.1111/j.1365-
535 246X.2007.03450.x (2007).

536 30 Gaina, C. *et al.* The African Plate: A history of oceanic crust accretion and subduction since the Jurassic.
537 *Tectonophysics* **604**, 4-25, doi:10.1016/j.tecto.2013.05.037 (2013).

538 31 Agard, P., Jolivet, L., Vrielynck, B., Burov, E. & Monié, P. Plate acceleration: The obduction trigger?
539 *Earth and Planetary Science Letters* **258**, 428-441, doi:10.1016/j.epsl.2007.04.002 (2007).

540 32 Jolivet, L. *et al.* Neo-Tethys geodynamics and mantle convection: from extension to compression in Africa
541 and a conceptual model for obduction. *Canadian journal of earth sciences* **53**, 1190-1204 (2015).

542 33 Stampfli, G. M. & Borel, G. A plate tectonic model for the Paleozoic and Mesozoic constrained by
543 dynamic plate boundaries and restored synthetic oceanic isochrons. *Earth and Planetary Science Letters*
544 **196**, 17-33 (2002).

545 34 van Hinsbergen, D. J. J. *et al.* Reconstructing Greater India: Paleogeographic, kinematic, and geodynamic
546 perspectives. *Tectonophysics* **760**, 69-94, doi:10.1016/j.tecto.2018.04.006 (2019).

547 35 Kapp, P. & DeCelles, P. G. Mesozoic–Cenozoic geological evolution of the Himalayan-Tibetan orogen and
548 working tectonic hypotheses. *American Journal of Science* **319**, 159-254 (2019).

549 36 Advokaat, E. L. *et al.* Early Cretaceous origin of the Woyla Arc (Sumatra, Indonesia) on the Australian
550 plate. *Earth and Planetary Science Letters* **498**, 348-361 (2018).

551 37 Plunder, A. *et al.* History of subduction polarity reversal during arc-continent collision: constraints from the
552 Andaman Ophiolite and its metamorphic sole. *Tectonics*, e2019TC005762 (2020).

553 38 Torsvik, T. *et al.* Late Cretaceous magmatism in Madagascar: palaeomagnetic evidence for a stationary
554 Marion hotspot. *Earth and Planetary Science Letters* **164**, 221-232 (1998).

555 39 Mohan, M. R. *et al.* The Ezhimala igneous complex, southern India: Possible imprint of late Cretaceous
556 magmatism within rift setting associated with India–Madagascar separation. *Journal of Asian Earth*
557 *Sciences* **121**, 56-71 (2016).

558 40 Cande, S. C. & Stegman, D. R. Indian and African plate motions driven by the push force of the Reunion
559 plume head. *Nature* **475**, 47-52, doi:10.1038/nature10174 (2011).

560 41 van Hinsbergen, D. J. J., Steinberger, B., Doubrovine, P. V. & Gassmöller, R. Acceleration and
561 deceleration of India-Asia convergence since the Cretaceous: Roles of mantle plumes and continental
562 collision. *Journal of Geophysical Research* **116**, doi:10.1029/2010jb008051 (2011).

563 42 Wang, Y. & Li, M. The interaction between mantle plumes and lithosphere and its surface expressions: 3-D
564 numerical modelling. *Geophysical Journal International*, doi:10.1093/gji/ggab014 (2021).

565 43 Kumar, P. *et al.* The rapid drift of the Indian tectonic plate. *Nature* **449**, 894-897, doi:10.1038/nature06214
566 (2007).

567 44 Lamb, S. & Davis, P. Cenozoic climate change as a possible cause for the rise of the Andes. *Nature* **425**,
568 792-797 (2003).

569 45 van der Meer, D. G., Spakman, W., van Hinsbergen, D. J. J., Amaru, M. L. & Torsvik, T. H. Towards
570 absolute plate motions constrained by lower-mantle slab remnants. *Nature Geoscience* **3**, 36-40,
571 doi:10.1038/ngeo708 (2010).

572 46 Tavani, S., Corradetti, A., Sabbatino, M., Seers, T. & Mazzoli, S. Geological record of the transition from
573 induced to self-sustained subduction in the Oman Mountains. *Journal of Geodynamics* **133**, 101674 (2020).
574 47 Tackley, P. J. Mantle convection and plate tectonics: Toward an integrated physical and chemical theory.
575 *Science* **288**, 2002-2007 (2000).
576 48 Coltice, N., Husson, L., Faccenna, C. & Arnould, M. What drives tectonic plates? *Science Advances* **5**,
577 eaax4295 (2019).
578 49 Dilek, Y. Ophiolite pulses, mantle plumes and orogeny. *Geological Society, London, Special Publications*
579 **218**, 9-19 (2003).
580 50 Ernst, R., Grosfils, E. & Mege, D. Giant dike swarms: Earth, venus, and mars. *Annual Review of Earth and*
581 *Planetary Sciences* **29**, 489-534 (2001).
582 51 Müller, R. D. *et al.* GPlates: building a virtual Earth through deep time. *Geochemistry, Geophysics,*
583 *Geosystems* **19**, 2243-2261 (2018).
584 52 Clube, T. M. M., Creer, K. M. & Robertson, A. H. F. Palaeorotation of the Troodos microplate, Cyprus.
585 *Nature* **317**, 522, doi:10.1038/317522a0 (1985).
586 53 Morris, A., Meyer, M., Anderson, M. W. & MacLeod, C. J. Clockwise rotation of the entire Oman
587 ophiolite occurred in a suprasubduction zone setting. *Geology* **44**, 1055-1058 (2016).
588 54 McQuarrie, N. & van Hinsbergen, D. J. J. Retrodeforming the Arabia-Eurasia collision zone: Age of
589 collision versus magnitude of continental subduction. *Geology* **41**, 315-318, doi:10.1130/g33591.1 (2013).
590 55 Monsef, I. *et al.* Evidence for an early-MORB to fore-arc evolution within the Zagros suture zone:
591 Constraints from zircon U-Pb geochronology and geochemistry of the Neyriz ophiolite (South Iran).
592 *Gondwana Research* **62**, 287-305 (2018).
593 56 Galoyan, G. *et al.* Geology, geochemistry and ⁴⁰Ar/³⁹Ar dating of Sevan ophiolites (Lesser Caucasus,
594 Armenia): evidence for Jurassic Back-arc opening and hot spot event between the South Armenian Block
595 and Eurasia. *Journal of Asian Earth Sciences* **34**, 135-153 (2009).
596 57 Çelik, Ö. F. *et al.* Jurassic metabasic rocks in the Kızılırmak accretionary complex (Kargı region, Central
597 Pontides, Northern Turkey). *Tectonophysics* **672-673**, 34-49, doi:10.1016/j.tecto.2016.01.043 (2016).
598 58 Topuz, G. *et al.* Jurassic ophiolite formation and emplacement as backstop to a subduction-accretion
599 complex in northeast Turkey, the Refahiye ophiolite, and relation to the Balkan ophiolites. *American*
600 *Journal of Science* **313**, 1054-1087, doi:10.2475/10.2013.04 (2014).
601 59 Ao, S. *et al.* U-Pb zircon ages, field geology and geochemistry of the Kermanshah ophiolite (Iran): From
602 continental rifting at 79Ma to oceanic core complex at ca. 36Ma in the southern Neo-Tethys. *Gondwana*
603 *Research* **31**, 305-318, doi:10.1016/j.gr.2015.01.014 (2016).
604 60 Peters, T. & Mercolli, I. Extremely thin oceanic crust in the Proto-Indian Ocean: Evidence from the
605 Masirah Ophiolite, Sultanate of Oman. *Journal of Geophysical Research: Solid Earth* **103**, 677-689,
606 doi:10.1029/97jb02674 (1998).
607 61 Gnos, E. *et al.* Bela oceanic lithosphere assemblage and its relation to the Reunion hotspot. *Terra Nova* **10**,
608 90-95 (1998).
609 62 Tapponnier, P., Mattauer, M., Proust, F. & Cassaigneau, C. Mesozoic ophiolites, sutures, and large-scale
610 tectonic movements in Afghanistan. *Earth and Planetary Science Letters* **52**, 355-371 (1981).
611 63 van Hinsbergen, D. J. J. *et al.* Greater India Basin hypothesis and a two-stage Cenozoic collision between
612 India and Asia. *Proc Natl Acad Sci U S A* **109**, 7659-7664, doi:10.1073/pnas.1117262109 (2012).
613 64 Yuan, J. *et al.* Rapid drift of the Tethyan Himalaya terrane before two-stage India-Asia collision. *National*
614 *Science Review* (2020).
615 65 Hébert, R. *et al.* The Indus-Yarlung Zangbo ophiolites from Nanga Parbat to Namche Barwa syntaxes,
616 southern Tibet: First synthesis of petrology, geochemistry, and geochronology with incidences on
617 geodynamic reconstructions of Neo-Tethys. *Gondwana Research* **22**, 377-397,
618 doi:10.1016/j.gr.2011.10.013 (2012).
619 66 Zahirovic, S. *et al.* Tectonic evolution and deep mantle structure of the eastern Tethys since the latest
620 Jurassic. *Earth-Science Reviews* **162**, 293-337 (2016).
621 67 Huang, W. *et al.* Lower Cretaceous Xigaze ophiolites formed in the Gangdese forearc: Evidence from
622 paleomagnetism, sediment provenance, and stratigraphy. *Earth and Planetary Science Letters* **415**, 142-
623 153, doi:10.1016/j.epsl.2015.01.032 (2015).
624 68 Westerweel, J. *et al.* Burma Terrane part of the Trans-Tethyan arc during collision with India according to
625 palaeomagnetic data. *Nature Geoscience* **12**, 863-868 (2019).
626 69 Jagoutz, O., Royden, L., Holt, A. F. & Becker, T. W. Anomalously fast convergence of India and Eurasia
627 caused by double subduction. *Nature Geoscience* **8**, 475-478, doi:10.1038/ngeo2418 (2015).

628 70 Höink, T. & Lenardic, A. Long wavelength convection, Poiseuille–Couette flow in the low-viscosity
629 asthenosphere and the strength of plate margins. *Geophysical Journal International* **180**, 23-33 (2010).
630 71 Höink, T., Jellinek, A. M. & Lenardic, A. Viscous coupling at the lithosphere-asthenosphere boundary.
631 *Geochemistry, Geophysics, Geosystems* **12** (2011).
632 72 Campbell, I. H. Testing the plume theory. *Chemical Geology* **241**, 153-176 (2007).
633 73 Doubrovine, P. V., Steinberger, B. & Torsvik, T. H. A failure to reject: Testing the correlation between
634 large igneous provinces and deep mantle structures with EDF statistics. *Geochemistry, Geophysics,*
635 *Geosystems* **17**, 1130-1163 (2016).
636 74 Steinberger, B. Topography caused by mantle density variations: observation-based estimates and models
637 derived from tomography and lithosphere thickness. *Geophysical Journal International* **205**, 604-621
638 (2016).
639 75 Steinberger, B. & Becker, T. W. A comparison of lithospheric thickness models. *Tectonophysics* **746**, 325-
640 338 (2018).
641